Article

An Optimization Study of Carbon Dioxide Absorption into the Aqueous Solution of Monoethanolamine and Tetrabutylphosphonium Methanesulfonate Hybrid Solvent Using RSM-CCD Methodology

Mus'ab Umair Zainul Anuar [1]**, Mohd Faisal Taha** [1,2,*]**, Noor Mona Md Yunus** [2]**, Siti Musliha Mat Ghani** [2] **and Azila Idris** [3,4]

[1] Fundamental and Applied Science Department, Universiti Teknologi PETRONAS, Seri Iskandar 32610, Perak, Malaysia; musab.umair_25122@utp.edu.my

[2] Centre of Research in Ionic Liquids, Universiti Teknologi PETRONAS, Seri Iskandar 32610, Perak, Malaysia; mona.yunus@utp.edu.my (N.M.M.Y.); siti_17007548@utp.edu.my (S.M.M.G.)

[3] University Malaya Centre of Ionic Liquids (UMCiL), University Malaya, Kuala Lumpur 50603, Malaysia; azila_idris@um.edu.my

[4] Department of Chemistry, Faculty of Science, University Malaya, Kuala Lumpur 50603, Malaysia

[*] Correspondence: faisalt@utp.edu.my; Tel.: +60-05-3687660

Abstract: The main purposes of this project are to assess and to optimize the solubility of carbon dioxide (CO_2) in an aqueous 30 wt% monoethanolamine-tetrabutylphosphonium methanesulfonate (MEA-[TBP][MeSO$_3$]) new hybrid solvent. In this study, the viscosity and density of aqueous MEA-[TBP][MeSO$_3$] hybrid solvents containing different amounts of [TBP][MeSO$_4$] were determined. Meanwhile, Fourier Transform-Infrared (FT-IR) Spectroscopy was used to determine the presence of carbamate in aqueous MEA-[TBP][MeSO$_3$] to prove that CO_2 was absorbed by aqueous MEA-[TBP][MeSO$_3$]. Response Surface Methodology (RSM) based on central composite design (CCD) was used to design the experiments and explore the effects of three independent parameters on the solubility of CO_2 in aqueous MEA-[TBP][MeSO$_3$]. The three independent parameters are concentration of [TBP][MeSO$_3$] (2–20 wt.%), temperature (30–60 °C) and pressure of CO_2 (2–30 bar). The experimental data was found to fit a quadratic equation using multiple regressions and analyzed using analysis of variance (ANOVA). The final empirical equation in terms of actual factors was deducted as mol fraction = $0.5316 - (2.76 \times 10^{-4})A - (8.8 \times 10^{-4})B + (8.48 \times 10^{-3})C + (2.9 \times 10^{-5})AB + (2.976 \times 10^{-6})AC + (5.5 \times 10^{-5})BC - (8.4 \times 10^{-5})A^2 - (3.3 \times 10^{-5})B^2 - (1.19 \times 10^{-4})C^2$, whereby A = ionic liquid ([TBP][MeSO$_3$]) concentration, B = temperature and C = CO_2 pressure. An attempt was made to perform the experiments for solubility of CO_2 in aqueous MEA-[TBP][MeSO$_3$] to validate the removal of CO_2 predicted by RSM. Based on a validation study, the experimental data showed a percentage error between 0.6% and 2.11% as compared to the predicted value of CO_2 removal by RSM.

Keywords: carbon dioxide; ionic liquid; absorption; Response Surface Methodology (RSM)

1. Introduction

The world is in the process of switching to more eco-friendly fuels that contain low carbon, such as natural gas (NG), for energy creation. NG is considered as a non-pollutant energy resource compared to fossil fuels and charcoal, and it is widely used in industrial and domestic applications due to its abundance and low cost. Although the demand for NG for 2020 dropped to 4% due to the COVID-19 pandemic, it was predicted that in 2021 demand will progressively recover [1,2]. NG collected offshore carries impurities such as CO_2, and it is known that NG contains 20% CO_2. CO_2 from NG feed gas forms carbamic acid with water vapor present in NG, and this acid can corrode pipelines and other equipment.

CO_2 also causes problems during the liquefaction of NG in multi-cryogenic heat exchange (MCHE) systems and affects the value of final liquefied natural gas (LNG) products [3,4]. In addition, CO_2 distributes zero heating value during combustion; therefore, it must be removed to meet the NG quality specifications before it can be handed over to variety of end-users. According to Rufford and colleagues, the specification of NG in pipelines distributed to customers is typically less than 3% CO_2 [4].

One of the most feasible methods to reduce CO_2 in the oil and NG industry is through chemical absorption. Currently, the chemical solvents that are widely used as CO_2 absorbents are aqueous alkanolamines, in which CO_2 is absorbed through the formation of a CO_2-amine complex mixture. The CO_2-amine complex mixture is then subjected to a 'stripping' process to release the CO_2 so it can be kept in CO_2 storage. This technology is known as the amine 'scrubbing' process and has been widely utilized as a CO_2 capture technology [3,5]. Currently, the commercial alkanolamines that are being used in the amine 'scrubbing' process are monoethanolamines (MEAs), methyldiethanolamines (MDEAs), and more recently, triethanolamines (TEAs) due to their re-activity with CO_2; they form stable carbamates as intermediates. However, amine CO_2 capture does suffer from many inherent drawbacks. The history of amine CO_2 capture systems shows that the system suffers from high equipment corrosion rates. Long-term corrosion effects can lead to increases in equipment downtime, loss of production, reduced equipment lifespan, injuries, or even death [6,7].

In the last 20 years, numerous studies have been conducted to improve carbon capture technology and solvent recoverability, many of which have emphasized the shortcomings of conventional aqueous alkanolamine solvents used in 'scrubbing' technology. As an alternative solution to overcome the disadvantages of conventional aqueous alkanolamine solvents, researchers have found that ionic liquids (ILs) are perfect candidates due to their high CO_2 solubility. ILs, often regarded as molten salts, are compounds that are completely made up of bulky ions and have a melting point below 100 °C [6,8,9]. They have remarkable properties such as negligible volatility, high thermal stability, non-flammability, tunability and solvation properties. Apart from this, ILs are attractive because of their tunable physicochemical properties. In 1999, initial research on CO_2 solubility in ILs conducted by Blanchard and colleagues showed that large amounts of CO_2 could be dissolved in imidazolium-based ionic liquids without contaminating the product used [10].

Despite having remarkable properties, ILs also have their drawbacks; these ultimately prevent them from being utilized by the industry. Generally, ILs have high viscosity and are expensive, making them not economically feasible to be used in large-scale production plants [6]. Thus, the addition of small amounts of ILs to aqueous alkanolamines to produce hybrid solvents is a better option, as this would utilize the advantages offered by both ILs and alkanolamines while suppressing their limitations. Considering the widespread use of amine CO_2 capture technology, the addition of small quantities of ionic liquid into aqueous alkanolamines would not create any significant changes in existing process designs [11].

Many of the inherent drawbacks were found to be addressed by the incorporation of ILs in aqueous amine solvents. For example, Hasib-Ur Rahman and his colleagues studied the corrosion effects of IL-alkanolamine hybrid solvents on carbon steel 1020. Their study showed a significant reduction (98% reduced) in the corrosion rate when IL-alkanolamine hybrid solvents were tested with carbon steel 1020. Their study also included the corrosion effects of CO_2 gas loading, effects of oxygen in the gas streams, effects of water content, and the effect of varying process conditions; the corrosion results were found to be significantly positive for IL-alkanolamine hybrid solvents [8]. Feng and Camper and colleagues studied the effects of ammonium-based ionic liquid incorporation in aqueous methyldiethanolamine (MDEA) on CO_2 absorption performance as well as solvent regeneration efficiency. Their studies showed that higher concentrations (0–30 wt%) of ionic liquid in MDEA increased CO_2 absorption rate as well as CO_2 absorption capacity. The effects of temperature have also been investigated; the CO_2 absorption capacity was only slightly affected with an increase in temperature (298K–318K) [5,12].

In this project, MEA and tetrabutylphosphonium methanesulfonate ([TBP][MeSO$_3$]) were selected to be mixed, producing aqueous hybrid solvent for CO_2 removal. The MEA concentration was kept constant at 30 wt% as per typical amine concentrations used in commercialized CO_2 absorption technology [13,14]. The selection of [TBP][MeSO$_3$] was based on the results of a screening study using the Conductor-like Screening Model for Real Solvents (COSMO-RS) by Azman [15]. His work aimed to determine ILs that can be mixed with aqueous alkanolamines to form hybrid solvents and to predict the capability of these ILs to capture CO_2. His findings revealed that phosphonium-based ILs showed relatively high CO_2 capacity in general and moderate cation-anion pairing. In addition, phosphonium-based ionic liquids are generally inexpensive and available commercially on a large scale [16]. The response surface methodology (RSM), based on central composite design (CCD), was employed to optimize and to comprehend the interactions between the operating factors affecting CO_2 removal using aqueous MEA-[TBP][MeSO$_3$] hybrid solvents with different concentrations of [TBP][MeSO$_3$].

2. Materials and Methods

2.1. Materials

Tetrabutylphosphonium methanesulfonate ([TBP][MeSO$_3$]) and monoethanolamine (MEA) were purchased from Merck. Carbon dioxide gas was purchased from Linde with a purity of 99.8%.

2.2. Density and Viscosity Measurement

The density of all the aqueous MEA-[TBP][MeSO$_3$] samples was measured using a Stabinger density viscosity meter (Anton Paar SVM3000, Anton Paar) with a precision of ± 0.0001 gcm^{-3}. All measurements of the density were performed at 30 °C, 45 °C and 60 °C. The viscosity of the aqueous MEA-[TBP][MeSO$_3$] samples were measured using a TA Instrument DHR-1 rheometer at 30 °C, 45 °C and 60 °C.

2.3. Solubility of CO_2 in Aqueous MEA-[TBP][MeSO$_3$]

The CO_2 solubility in the aqueous MEA-[TBP][MeSO$_3$] sample was carried out based on the isochoric saturation method [17]. A high-pressure equilibrium cell (EC) with a capacity of 15 mL made of stainless steel was used to carry out the experiments. The equilibrium cell was attached with a pressure gauge and temperature controller having ranges from 0 to 40 bar and a room temperature of 80 °C, respectively. The schematic of the experimental setup is shown in Figure 1. The temperature inside the equilibrium cell was maintained by a water bath. A pressure gauge was used to measure the pressure inside the system.
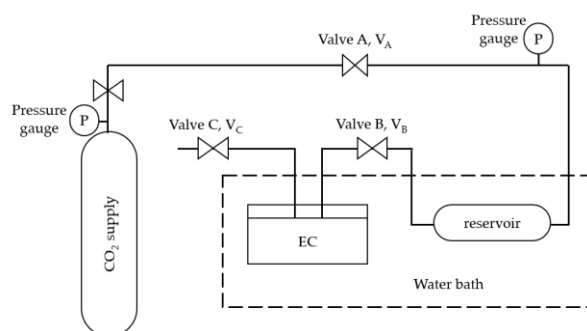

Figure 1. Schematic diagram of CO_2 absorption apparatus.

During the experiment, a known quantity of aqueous MEA-[TBP][MeSO$_3$] was loaded into the equilibrium cell (EC). The EC was degassed by a vacuum pump and the desired temperature inside the EC was maintained using a chiller. CO_2 gas was then introduced into the reservoir of known volume (from V_A to V_B) and brought to a constant temperature

in order to calculate the initial number of moles of CO_2 before sending to the EC. The initial number of moles of CO_2 was calculated using Equation (1).

$$n^i_{CO_2} = \frac{P_i V_{res}}{Z^i_{CO_2} R T_i} \tag{1}$$

where $n^i_{CO_2}$ is the initial number of moles of CO_2 charged into EC, P_i is the initial pressure, T_i is the initial temperature, V_{res} is the volume of the reservoir, $Z^i_{CO_2}$ is the compressibility factor at initial temperature and pressure conditions (calculated from Peng-Robinson equation of state) and R is the universal gas constant.

CO$_2$ was then introduced into EC by opening V_B. As the absorption of CO_2 in aqueous MEA-[TBP][MeSO$_3$] starts, the pressure inside the cell reduces in continuous manner. The pressure in the system was recorded in 1 min intervals, as the whole system was allowed sufficient time to reach the equilibrium. The time duration varied between 90 and 120 min. At the equilibrium condition, the moles of CO_2 left in the cell were calculated using Equation (2).

$$n^{eq}_{CO_2} = \frac{P_{eq}(V_{total} - V_s)}{Z^f_{CO_2} R T_{eq}} \tag{2}$$

where $n^{eq}_{CO_2}$ is the number of moles of CO_2 left in the system at equilibrium, P_{eq} is the pressure at equilibrium, T_{eq} is the temperature at equilibrium, V_{total} is the volume of the CO_2 absorption system from valve A (V_A) to valve C (V_C), V_s is volume of aqueous MEA-[TBP][MeSO$_3$] and $Z^f_{CO_2}$ is the compressibility factor at equilibrium temperature and pressure conditions (calculated from Peng-Robinson equation of state). The number of moles of CO_2 absorbed ($n^{abs}_{CO_2}$) by aqueous MEA-[TBP][MeSO$_3$] is given by Equation (3).

$$n^{abs}_{CO_2} = n^{eq}_{CO_2} - n^i_{CO_2} \tag{3}$$

where $n^{eq}_{CO_2}$ is the number of moles of CO_2 left in the system at equilibrium and $n^i_{CO_2}$ is the initial number of moles of CO_2 charged into EC. Meanwhile, the solubility of CO_2 expressed in mole fraction (x_2) was calculated according to Equation (4).

$$x_2 = \frac{n^{abs}_{CO_2}}{n^{abs}_{CO_2} + n_s} \tag{4}$$

where $n^{abs}_{CO_2}$ is the number of moles of CO_2 absorbed by aqueous MEA-[TBP][MeSO$_3$] and n_s is the number of moles of aqueous MEA-[TBP][MeSO$_3$] used in the system.

2.4. Optimization Study of CO$_2$ Solubility in the Aqueous MEA-[TBP][MeSO$_3$] Solvent Using RSM

The response surface methodology (RSM) was developed based on the central composite design (CCD), with CO_2 as the dependent variable (responses), using Design-Expert software version 12. The factors of experimental design, including IL ([TBP][MeSO$_3$]) concentration (wt%), temperature (°C) and pressure of CO_2 (bar), were selected. The CCD was performed using a 2^3 face centered design and, according to the three levels and three variable concepts, 20 experimental points in random order were adopted in this design. The three independent variables were prescribed into three levels (low, basal and high) and coded values (−1, 0, +1). CCD was chosen because the design includes a repetition of center points that is used to calculate the experimental error, providing more reliable data. A total of 20 runs of experiments were performed, and the experimental results were fitted to regression model equation.

In this study, the independent variable for the IL (TBP][MeSO$_3$]) concentration was represented by variable A, while the temperature was denoted as B and the pressure of CO_2 was denoted as C. The range and levels of the processing parameters involved are shown in Table 1.

Table 1. Independent variables and concentration levels for response surface study.

Factors	Unit	Levels		
		−1	0	+1
A: IL ([TBP][MeSO$_3$]) concentration	wt%	2	10	20
B: Temperature	°C	30	45	60
C: Pressure of CO$_2$	bar	2	16	30

2.5. FT-IR Spectroscopy

FT-IR analysis was carried out for aqueous MEA, aqueous 20 wt% [TBP][MeSO$_3$] and aqueous MEA-[TBP][MeSO$_3$], before and after their exposure to CO$_2$, with the main purpose of identifying new bands of the carbamate species that show that CO$_2$ is chemically absorbed by the samples as amine reacts with CO$_2$ to form carbamate [18]. Each spectrum was recorded in spectral ranging from 4000 to 550 cm^{-1}.

3. Results

3.1. Density and Viscosity

The effect of IL ([TBP][MeSO$_3$]) concentration and temperature on the density of aqueous MEA-[TBP][MeSO$_3$] solvent was studied. Figure 2 shows the significant effect of IL concentration and temperature on the density of the hybrid solvents. As expected, the density of the aqueous MEA-[TBP][MeSO$_3$] solvent increased with the increased of IL concentration due to more molecules present in the hybrid solvent at constant volume. The aqueous MEA, without the presence of IL, showed the lowest density as compared to the hybrid solvents. Meanwhile, as expected, the density of the hybrid solvent was found to be decreased by increasing the temperature. This is due to the increase in volume, as heat causes the molecules to move faster and move apart as they receive the high kinetic energy of the increasing temperature, which in turn reduces the density.
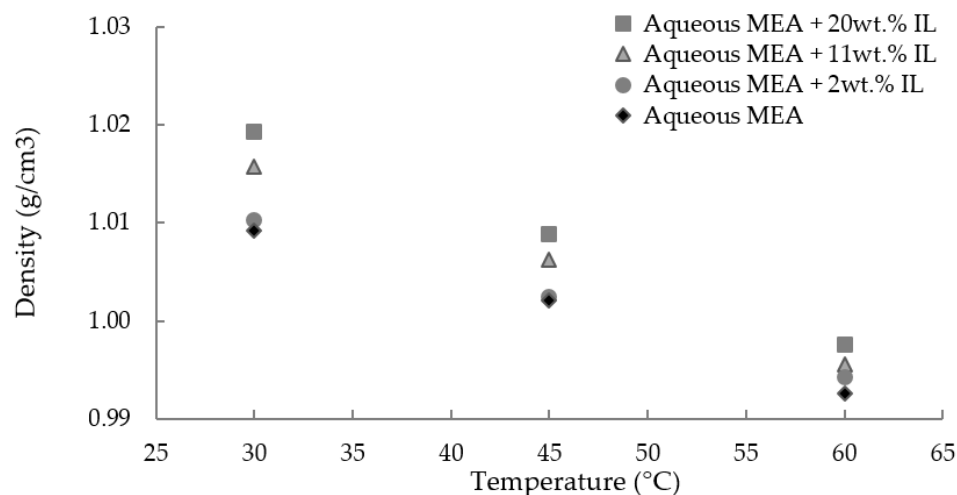

Figure 2. Density of aqueous MEA and aqueous MEA-[TBP][MeSO$_3$] solvent at different IL concentrations and temperatures.

The effect of IL concentration and temperature on the viscosity of aqueous MEA-[TBP][MeSO$_3$] solvent was studied. Figure 3 presents the plot graph of viscosity of the hybrid solvent with different concentrations of IL and at different temperatures. As shown in the figure, the viscosity of all absorbents used in this study was low (less than 0.05 Pa.s), which could help facilitate the mass transfer for CO$_2$ absorption [13]. Figure 3 also demonstrates, as expected, that the viscosity of the hybrid solvent decreases with increasing temperature. Higher thermal energy causes the molecules to become more mobile and weakens the molecular resistance. Meanwhile, the increase in concentration of

IL causes the increase of the internal resistance in the mixture, which in turn increases the viscosity of the hybrid solvent [19].
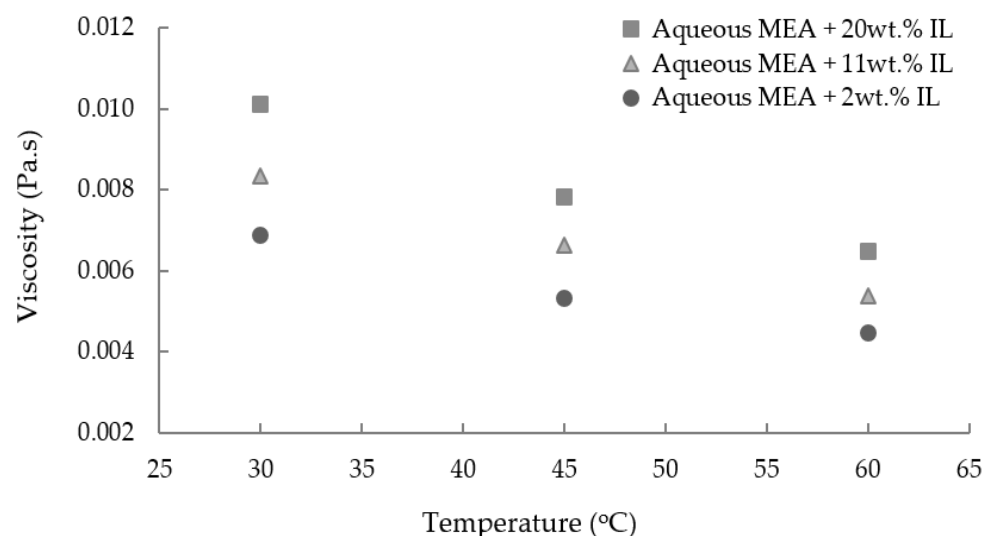

Figure 3. Viscosity of aqueous MEA-[TBP][MeSO$_3$] solvent at different IL concentrations and temperatures.

3.2. FT-IR Spectroscopy

Figure 4 shows the FT-IR spectrum in the region from 800 to 1800 cm^{-1} for samples before and after the CO$_2$ solubility experiment, while Table 2 shows important band assignment analysis of the FT-IR spectra. The wavenumber regions from 650 to 800 cm^{-1} and from 1800 to 4000 cm^{-1} do not provide useful information for interaction between samples and CO$_2$. In Figure 4a, no new band emergence was observed for 20 wt.% [TBP][MeSO$_3$] aqueous sample after CO$_2$ exposure, indicating physical absorption of CO$_2$ in the aqueous IL [10]. As shown in Figure 4b,c, emergence of new bands at 1568, 1486 and 1312 cm^{-1} was observed in the sample of aqueous MEA and aqueous MEA-[TBP][MeSO$_3$] after the CO$_2$ solubility experiment. These bands are assigned to carbamate's COO$^-$ asymmetric and COO$^-$ symmetric stretching and N-COO$^-$ stretching vibration. It should be noted that the bands at 955 cm^{-1} (C-N-H out-of-plane wagging and C-NH$_2$ twisting) and 1362 cm^{-1} (NH$_2$ twisting) for MEA in the samples decreased upon CO$_2$ exposure. There was also protonation of MEA, resulting in a C-N stretching mode shift from 1074 to 1066 cm^{-1}. Similar observations where stable carbamate is formed when MEA reacted with CO$_2$ have been reported [18,20,21]. This chemical bonded formation can lead to large amounts of energy required for regeneration of the amine [4].

Table 2. FT-IR absorption band assignment.

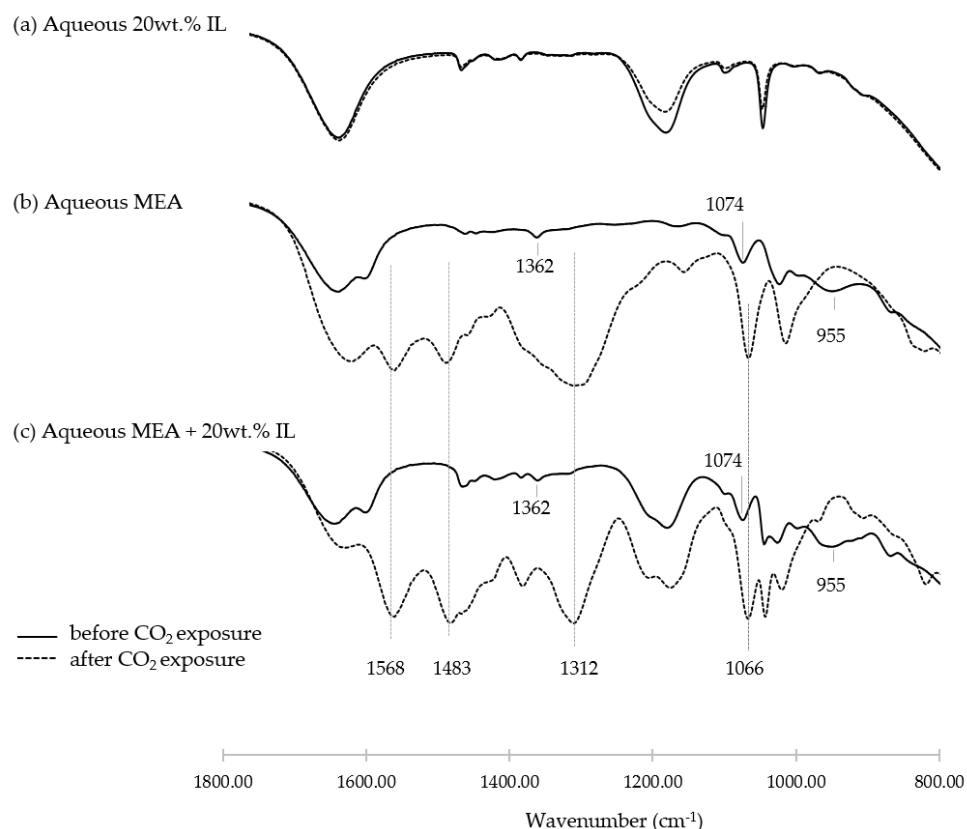| Band (cm^{-1})	Assignment
1568	COO$^-$ (carbamate)
1483	COO$^-$ (carbamate)
1380	C-O (CO$_2$/ CO$_3^{2-}$ physical adsorption)
1362	NH$_2$ (MEA)
1312	N-COO$^-$ (carbamate)
1074	C-N stretching (MEA)
1066	C-N (protonated MEA, carbamate)
955	C-NH$_2$ (MEA)

Figure 4. FT-IR spectra of samples: (**a**) aqueous 20 wt% of IL; (**b**) aqueous 30 wt% of MEA and (**c**) aqueous MEA + 20 wt% IL before (solid line) and after (dash line) exposure to CO_2.

3.3. Optimization Study of CO_2 Solubility in the Aqueous MEA-[TBP][MeSO₃] Solvent Using RSM

In this study, response surface methodology (RSM) based on the central composite design (CCD) was employed to analyze the effects of three parameters, i.e. IL [TBP][MeSO₃] concentration, temperature and CO_2 pressure, on the absorption of CO_2 in aqueous MEA-[TBP][MeSO₃] solvent. The CCD was performed using a 2^3 face centered design according to the three levels and three variable concepts, in which 20 experimental runs in random order were adopted. Table 3 shows the parameters of each run that were generated using the central composite design (CCD) method and the experimental response data, which were degree CO_2 solubility in hybrid solvent.

3.3.1. Analysis of Variance (ANOVA)

The ANOVA analysis as presented in Table 4 indicates that the quadratic model is significant to represent the CO_2 removal using the aqueous MEA-[TBP][MeSO₃] solvent. The regression model is as follows:

$$\begin{aligned} \text{Mol fraction} = {} & 0.5316 - (2.76 \times 10^{-4})A - (8.8 \times 10^{-4})B + (8.48 \times 10^{-3})C \\ & + (2.9 \times 10^{-5})AB + (2.976 \times 10^{-6})AC + (5.5 \times 10^{-5})BC - (8.4 \times 10^{-5})A^2 \\ & - (3.3 \times 10^{-5})B^2 - (1.19 \times 10^{-4})C^2 \end{aligned} \quad (5)$$

As can be seen in Table 4, the calculated F-value of 90.84 and *p*-value <0.0001 indicate that the model was significant with low probability of error in this study. Correspondingly, the calculated lack of fit was 4.87, which was not significantly relative to the pure error. A possibility of 5.36% of large lack of fit F-value may occur due to noise. *p*-values less than 0.0500 indicate model terms are significant [22]. In this case B, C, BC and C^2 are significant model terms. The most significant model term was pressure, with the highest F-value of

668.98. The factor of IL concentration (A), with *p*-value of 0.0985, does not give significant effect towards the CO_2 solubility response.

Table 3. Experimental layout and results of 2^3 face centered central composite design.

Standard	A: IL Concentration (wt%)	B: Temperature (°C)	C: CO_2 Pressure (bar)	Mol Fraction	
				Experimental	Predicted
1	2	30	2	0.505	0.496
2	20	30	2	0.463	0.474
3	2	60	2	0.373	0.387
4	20	60	2	0.382	0.380
5	2	30	30	0.670	0.674
6	20	30	30	0.665	0.653
7	2	60	30	0.620	0.611
8	20	60	30	0.595	0.605
9	2	45	16	0.573	0.573
10	20	45	16	0.565	0.559
11	11	30	16	0.598	0.604
12	11	60	16	0.539	0.526
13	11	45	2	0.462	0.448
14	11	45	30	0.643	0.650
15	11	45	16	0.573	0.572
16	11	45	16	0.564	0.572
17	11	45	16	0.560	0.572
18	11	45	16	0.578	0.572
19	11	45	16	0.577	0.572
20	11	45	16	0.569	0.572

Table 4. ANOVA for quadratic modelling of CO_2 removal.

Source	Sum of Squares	dF	Mean Square	F-Value	*p*-Value	
Model	0.1242	9	0.0138	90.84	<0.0001	significant
A-IL Concentration	0.0005	1	0.0005	3.32	0.0985	
B-Temp	0.0154	1	0.0154	101.17	<0.0001	
C-Pressures	0.1016	1	0.1016	668.98	<0.0001	
AB	0.0001	1	0.0001	0.7909	0.3947	
AC	1.125×10^{-6}	1	1.125×10^{-6}	0.0074	0.9331	
BC	0.0011	1	0.0011	7.12	0.0236	
A^2	0.0001	1	0.0001	0.8417	0.3805	
B^2	0.0001	1	0.0001	0.9697	0.3480	
C^2	0.0015	1	0.0015	9.84	0.0106	
Residual	0.0015	10	0.0002			
Lack of Fit	0.0013	5	0.0003	4.87	0.0536	not significant
Pure Error	0.0003	5	0.0001			
Cor Total	0.1257	19				

3.3.2. Fit Statistics

Fit summary output analysis showed that the quadratic model was statistically significant to represent the mol fraction of CO_2 solubility response (Table 5). The high value of R^2 (0.9879) indicates that the data fit the model very well. The predicted R^2 (0.8443) was in acceptable agreement with the adjusted R^2 (0.9770), as the difference was less than 0.2.

Table 5. Fit statistics of Response Surface Quadratic Model.

Factors	Value
Std. Dev.	0.0123
Mean	0.5537
Coefficient of variance percentage	2.23
R^2	0.9879
Adjusted R^2	0.9770
Predicted R^2	0.8443
Adequate Precision	33.7600

Figure 5a shows the actual against the predicted value plot for CO_2 solubility, where the residuals were generally placed on a straight line and normally distributed. The actual value and predicted values for all responses were close to each other, as shown in Table 3. These results confirmed that the predicted and actual values were in good agreement, with high acceptability of the models [23]. The adequate precision measures the signal to noise ratio, and the ratio value of 33.76 indicated an adequate signal (adeq precision >4) [24].
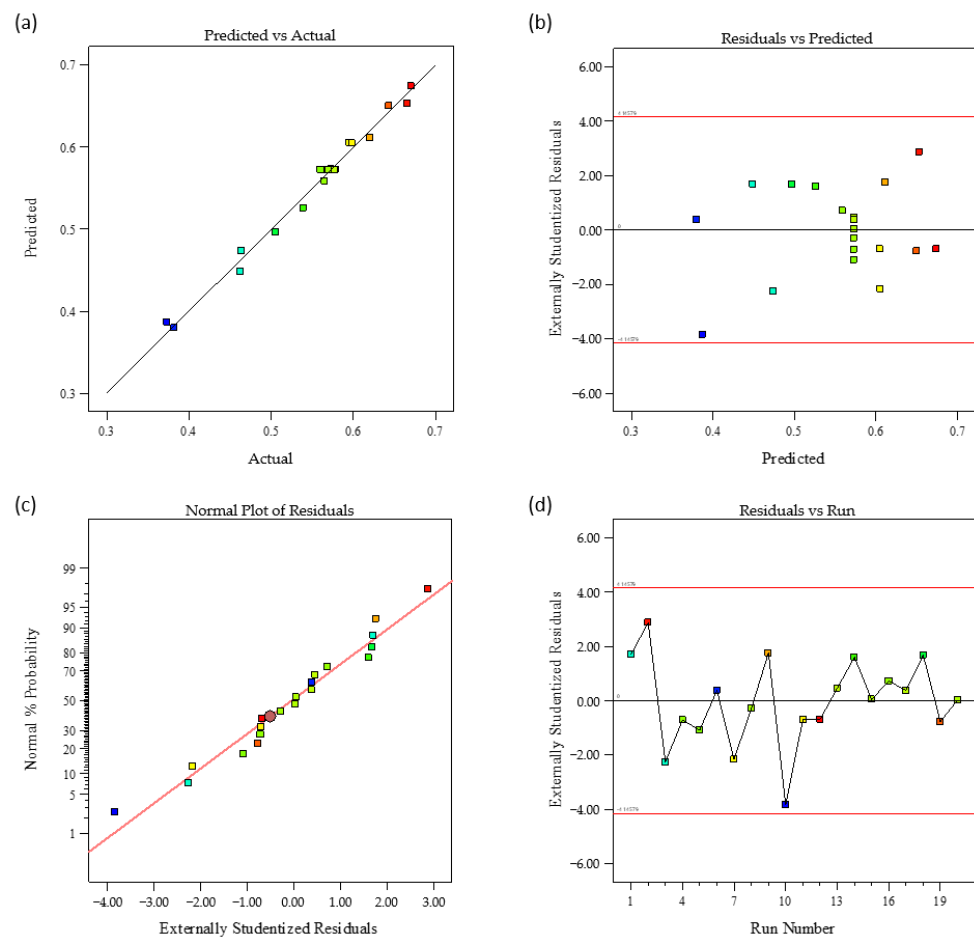

Figure 5. The CCD predicted value of CO_2 removal efficiency vs. (**a**) actual absorption and (**b**) externally studentized residuals, and externally studentized residuals vs. (**c**) normal probability and (**d**) experiment run number.

Figure 5b shows the residuals were equally dispersed inside the red line of the x-axis without any trend. This scenario suggested the proposed models were acceptably free from any violation of the independence or constant variance assumption. Figure 5c presents an analysis of the normal probability plot of residuals that provides additional info on the adequacy of the final model. The graph shows approximately linear residual distribution,

which indicates uniform distribution of errors. Thus, the adequacy of the least-square fit was justified. Meanwhile, Figure 5d shows the residual plots vs. experimental run order for CO_2 solubility in aqueous MEA-[TBP][MeSO$_3$] solvent. As can be seen in the plot, there is a random scatter, providing assurance that no other lurking variables may have influenced the response during the experiment.

3.3.3. Effect of the Variable Factors

The effect of the variable factors and their interactions on CO_2 solubility is shown in Figure 6. As seen in the perturbation plot in Figure 6a, temperature (curve B) and pressure (curve C) are the significant factors affecting the CO_2 solubility as compared to IL concentration (curve A). The analysis of variance summarized in Table 4 confirms these findings. Similar observations on the effect of IL addition into amine solution on CO_2 solubility have been reported. Xu et al. suggest that the absorption of CO_2 relies mainly on MEA, with little effect from IL, since adding salt might reduce the solubility of carbamate (resulting in MEA reacting with water) in a solution and hinder CO_2 absorption. This process is known as the salting out effect. Despite the reduced CO_2 solubility performance from the effect of IL concentration, the presence of IL may help in saving the energy during the regeneration process due to its lower heat capacity [13]. However, this work mainly focusses on the CO_2 absorption of this hybrid solvent, and further study on the desorption process will be necessary in the future.
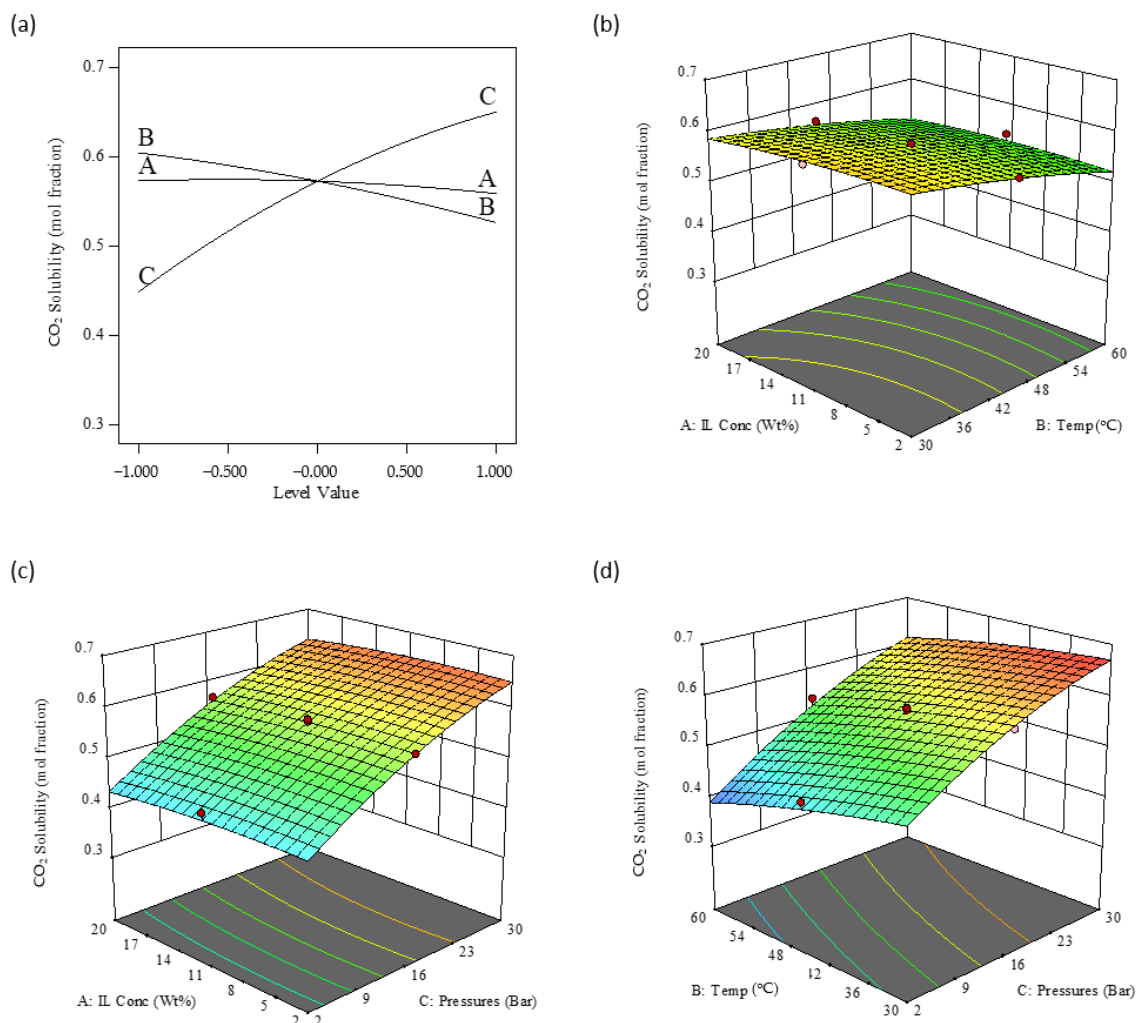

Figure 6. (**a**) Perturbation plot showing the effect of variable factors on CO_2 solubility and the response surface plots of CO_2 solubility as a function of (**b**) IL concentration and temperature, (**c**) IL concentration and pressure, and (**d**) pressure and temperature.

From the perturbation plot, it is seen that an increase in temperature decreases the CO_2 solubility, while an increase in pressure improves CO_2 solubility; this is a trend that is consistent with gas solubility in ILs. As CO_2 absorption involves an exothermic reaction, the chemisorption reaction decreases as the temperature increases. On the other hand, increasing the pressure of the gas increases the number of collisions between the CO_2 molecules and the surface of the solution; hence, more gas is dissolved as the pressure increases [25,26]. It can be seen from the perturbation plot and the 3D response surface plots that pressure has the highest effect on CO_2 solubility. RSM analyses also showed that no significant interactions took place between IL concentration and temperature, as shown in Figure 6b, and between IL concentration and pressure, as shown in Figure 6c. A significant interaction between temperature and pressure was detected, as seen in Figure 6d, which was indicated in the ANOVA table (Table 4). At high pressure, the effect of temperature on CO_2 solubility was higher compared to the effect of temperature on CO_2 solubility at lower pressure.

3.3.4. Validation of Empirical Model Adequacy

To ensure the developed empirical model was accurate, three validation experiments were implemented with new parameters, which were not tested during this experiment. The new parameters shown in Table 6 are within the ranges tested previously. The error ranging from 0.46% to 3.59% is within the 95% confidence interval. Hence, the model is acceptable, since the error is below 5.0%. The cause of error might be from random error.

Table 6. Results of operating conditions with experimental design in confirmation runs.

Run Factor			Mol Fraction		
A: IL Concentration (wt%)	B: Temperature (°C)	C: CO_2 Pressure (bar)	Actual	Predicted	Error (%)
20	30	16	0.579	0.594	2.53
20	45	2	0.439	0.437	0.46
20	45	30	0.617	0.640	3.59

3.3.5. Optimization of CO_2 Capture

Table 7 shows the optimized parameter values to achieve maximum CO_2 solubility in aqueous MEA-[TBP][MeSO$_3$] solvent. Based on the suggested RSM model, the predicted maximum mol fraction of CO_2 solubility in aqueous MEA-[TBP][MeSO$_3$] solvent under optimum conditions is 0.670. This value was only slightly higher as compared to the solubility of CO_2 in 30 wt% aqueous MEA solution, where the mol fraction of CO_2 solubility was found to be 0.613 under the same temperature and pressure conditions.

Table 7. Optimized condition for CO_2 solubility in aqueous MEA-[TBP][MeSO$_3$] solvent.

Factors	Value
[TBP][MeSO$_3$] concentration	2.093 wt%
Temperature	30.36 °C
Pressure	29.89 bar

4. Conclusions

An absorption study of CO_2 using an aqueous MEA-[TBP][MeSO$_3$] hybrid solvent under different IL concentrations, temperatures and pressures was conducted. The density and viscosity showed an increasing trend at high IL concentration and a decreasing trend with increasing temperature. The FT-IR spectroscopy analyses show physical absorption of CO_2 in [TBP][MeSO$_3$], while chemical absorption of CO_2 was detected in aqueous MEA and the hybrid solvents. The solubility CO_2 study using RSM concluded that the most significant factor in CO_2 solubility is pressure, followed by temperature. The IL

concentration did not have a significant effect on the mol fraction of CO_2 solubility. The validation of the experiment shows the quadratic model equation is within the acceptable range of error.

Institutional Review Board Statement: Not applicable.

Informed Consent Statement: Not applicable.

Conflicts of Interest: The authors declare no conflict of interest. The funders had no role in the design of the study; in the collection, analyses, or interpretation of data; in the writing of the manuscript, or in the decision to publish the results.

References

1. Gas 2020. Available online: https://www.iea.org/reports/gas-2020 (accessed on 4 April 2021).
2. Haider, J.; Saeed, S.; Qyyum, M.A.; Kazmi, B.; Ahmad, R.; Muhammad, A.; Lee, M. Simultaneous capture of acid gases from natural gas adopting ionic liquids: Challenges, recent developments, and prospects. *Renew. Sustain. Energy Rev.* **2020**, *123*, 109771. [CrossRef]
3. Rochelle, G.T. Amine Scrubbing for CO_2 Capture. *Science* **2009**, *325*, 1652–1654. [CrossRef]
4. Rufford, T.; Smart, S.; Watson, G.; Graham, B.; Boxall, J.; da Costa, J.D.; May, E. The removal of CO_2 and N_2 from natural gas: A review of conventional and emerging process technologies. *J. Pet. Sci. Eng.* **2012**, *94–95*, 123–154. [CrossRef]
5. Feng, Z.; Cheng-Gang, F.; You-Ting, W.; Yuan-Tao, W.; Ai-Min, L.; Zhi-Bing, Z. Absorption of CO_2 in the aqueous solutions of functionalized ionic liquids and MDEA. *Chem. Eng. J.* **2010**, *160*, 691–697. [CrossRef]
6. Vega, F.; Cano, M.; Camino, S.; Fernández, L.M.G.; Portillo, E.; Navarrete, B. Solvents for carbon dioxide capture. In *Carbon Dioxide Chemistry, Capture and Oil Recovery*; Karamé, I., Ed.; IntechOpen: London, UK, 2018; p. 142.
7. Veawab, A.; Tontiwachwuthikul, P.; Chakma, A. Corrosion Behavior of Carbon Steel in the CO_2 Absorption Process Using Aqueous Amine Solutions. *Ind. Eng. Chem. Res.* **1999**, *38*, 3917–3924. [CrossRef]
8. Hasib-Ur-Rahman, M.; Bouteldja, H.; Fongarland, P.; Siaj, M.; Larachi, F. Corrosion Behavior of Carbon Steel in Alkanolamine/Room-Temperature Ionic Liquid Based CO_2 Capture Systems. *Ind. Eng. Chem. Res.* **2011**, *51*, 8711–8718. [CrossRef]
9. Ramdin, M.; De Loos, T.W.; Vlugt, T.J. State-of-the-Art of CO_2 Capture with Ionic Liquids. *Ind. Eng. Chem. Res.* **2012**, *51*, 8149–8177. [CrossRef]
10. Blanchard, L.A.; Hancu, D.; Beckman, E.J.; Brennecke, J.F. Green processing using ionic liquids and CO_2. *Nature* **1999**, *399*, 28–29. [CrossRef]
11. Shojaeian, A.; Haghtalab, A. Solubility and density of carbon dioxide in different aqueous alkanolamine solutions blended with 1-butyl-3-methylimidazolium acetate ionic liquid at high pressure. *J. Mol. Liq.* **2013**, *187*, 218–225. [CrossRef]
12. Camper, D.; Bara, J.E.; Gin, D.L.; Noble, R.D. Room-Temperature Ionic Liquid−Amine Solutions: Tunable Solvents for Efficient and Reversible Capture of CO_2. *Ind. Eng. Chem. Res.* **2008**, *47*, 8496–8498. [CrossRef]
13. Xu, F.; Gao, H.; Dong, H.; Wang, Z.; Zhang, X.; Ren, B.; Zhang, S. Solubility of CO_2 in aqueous mixtures of monoethanolamine and dicyanamide-based ionic liquids. *Fluid Phase Equilibria* **2014**, *365*, 80–87. [CrossRef]
14. Liu, Y.; Dai, Z.; Dai, F.; Ji, X. Ionic Liquids/Deep Eutectic Solvents-Based Hybrid Solvents for CO_2 Capture. *Crystals* **2020**, *10*, 978. [CrossRef]
15. Azman, M.A.S. *Investigation on the CO_2 Solubility of Alkanolamine-ionic Liquid Hybrid Solvent*; Final Year Project; Universiti Teknologi Petronas: Seri Iskandar, Malaysia, 2020.
16. Stolarska, O.; Soto, A.; Rodríguez, H.; Smiglak, M. Properties modification by eutectic formation in mixtures of ionic liquids. *RSC Adv.* **2015**, *5*, 22178–22187. [CrossRef]
17. Palgunadi, J.; Kang, J.; Cheong, M.; Kim, H.; Lee, H. Fluorine-Free Imidazolium-Based Ionic Liquids with a Phosphorous-Containing Anion as Potential CO_2 Absorbents. *Bull. Korean Chem. Soc.* **2009**, *30*, 1749–1754. [CrossRef]
18. Sun, C.; Dutta, P.K. Infrared Spectroscopic Study of Reaction of Carbon Dioxide with Aqueous Monoethanolamine Solutions. *Ind. Eng. Chem. Res.* **2016**, *55*, 6276–6283. [CrossRef]
19. Khan, S.N.; Hailegiorgis, S.M.; Man, Z.; Shariff, A.M.; Garg, S. Thermophysical Properties of Aqueous 1-Butyl-3-Methylimidazolium Acetate [BMIM] [AC] + Monoethanolamine (MEA) Hybrid as a Solvent for CO_2 Capture. *Procedia Eng.* **2016**, *148*, 1326–1331. [CrossRef]
20. Cheng, H.; Song, H.; Toan, S.; Wang, B.; Gasem, K.A.; Fan, M.; Cheng, F. Experimental investigation of CO_2 adsorption and desorption on multi-type amines loaded HZSM-5 zeolites. *Chem. Eng. J.* **2021**, *406*, 126882. [CrossRef]

21. Ma, C.; Pietrucci, F.; Andreoni, W. Capturing CO_2 in Monoethanolamine (MEA) Aqueous Solutions: Fingerprints of Carbamate Formation Assessed with First-Principles Simulations. *J. Phys. Chem. Lett.* **2014**, *5*, 1672–1677. [CrossRef]

22. Morero, B.; Groppelli, E.S.; Campanella, E.A. Evaluation of biogas upgrading technologies using a response surface methodology for process simulation. *J. Clean. Prod.* **2017**, *141*, 978–988. [CrossRef]

23. Abdulredha, M.M.; Hussain, S.A.; Abdullah, L.C. Optimization of the demulsification of water in oil emulsion via non-ionic surfactant by the response surface methods. *J. Pet. Sci. Eng.* **2020**, *184*, 106463. [CrossRef]

24. Pashaei, H.; Ghaemi, A.; Nasiri, M.; Karami, B. Experimental Modeling and Optimization of CO_2 Absorption into Piperazine Solutions Using RSM-CCD Methodology. *ACS Omega* **2020**, *5*, 8432–8448. [CrossRef] [PubMed]

25. Shariff, A.; Shaikh, M.S.; Bustam, M.; Garg, S.; Faiqa, N.; Aftab, A. High-pressure Solubility of Carbon Dioxide in Aqueous Sodium L-Prolinate Solution. *Procedia Eng.* **2016**, *148*, 580–587. [CrossRef]

26. Maginn, E. *Ionic Liquids: Breakthrough Absorption Technology for Post-Combustion CO_2 Capture*; Technical Report; Office of Scientific and Technical Information (OSTI): Oak Ridge, TN, USA, 2012.